THE JOURNAL OF PHYSICAL CHEMISTRY C

Article

Cite This: J. Phys. Chem. C 2018, 122, 16048−16059

pubs.acs.org/JPCC

Chemical Dynamics Simulations and Scattering Experiments for O_2 Collisions with Graphite

Moumita Majumder,[†] K. D. Gibson,[‡] S. J. Sibener,[‡] and William L. Hase*,[†]

[†]Department of Chemistry and Biochemistry, Texas Tech University, Lubbock, Texas 79409, United States

[‡]The James Franck Institute and Department of Chemistry, The University of Chicago, 929 East 57th Street, Chicago, Illinois 60637, United States

ABSTRACT: Energy transfer in collisions of O_2 with a graphite surface was studied by chemical dynamics simulations. The simulations were performed for three collision energies E_i of 2.1, 7.4, and 15 kcal/mol, with the initial incident angle fixed at θ_i = 45°. Simulations were performed for each E_i at a surface temperature T_{surf} = 300 K. For the higher surface temperature of 1177 K, a simulation was only performed for E_i = 15 kcal/mol. The following properties were determined and analyzed for the O_2 + graphite collisions: (1) translational energy distributions of the scattered O_2; (2) distribution of the final polar and azimuthal angle for the scattered O_2; and (3) number of bounces of O_2 on the surface before scattering. The average energy transferred to the graphite surface and that remaining in O_2 translation, i.e., $\langle \Delta E_{surf} \rangle$ and $\langle E_f \rangle$, exhibit a linear dependence with the initial translational energy. For the O_2 + graphite scattering, the physisorption/desorption residence time distribution decays exponentially, with an increase in residence time with a decrease in E_i. The rate at which the distribution decreases shows a near-linear dependence with an increase in E_i. For higher collisional energies of 7.4 and 15 kcal/mol, O_2 scattering from the surface follows a nearly quasi-trapping desorption process. However, for the lowest collision energy, it mostly follows conventional physisorption/desorption. For all of the scattering conditions considered experimentally, the relationship between the average final translational energy and average scattering angle for the O_2 molecules found from the simulations is in excellent agreement with the experimental results. This experimental validation of precise simulation outcomes is important as it indicates that collisional energy-transfer predictions for this system can be reliably used in assessing interfacial energy flow in a variety of technological applications, including high-performance flight systems.

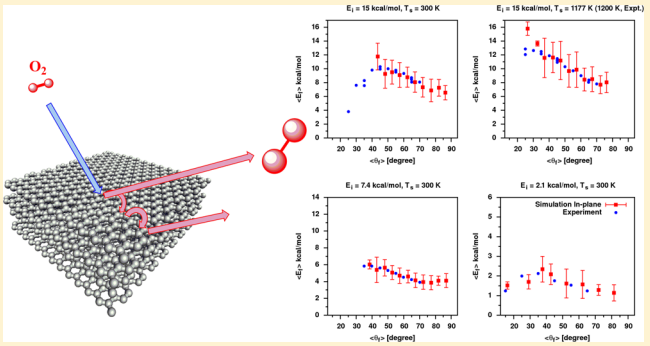

I. INTRODUCTION

Understanding energy-transfer dynamics at the gas−surface interface[1−5] provides fundamental information needed for accurate modeling of many chemical and physical phenomena. The energy-transfer dynamics for collisions of gas molecules with a surface is a complicated process, dependent on a number of properties, including the gas−surface potential, translational energy and incident angle of the projectile, gas−surface mass ratio, and surface temperature.

Gas−surface collision dynamics have been investigated for a variety of surfaces both theoretically and experimentally, including both organic[6−13] and metal surfaces.[14,15] A particularly interesting and important surface is graphite. It is one of the most prevalent carbon allotropes and has a layered and planar structure,[16,17] with the individual layers called graphene. The carbon atoms in each layer are arranged in a honeycomb lattice with a C−C bond distance of 1.42 Å.[16,17] The layers are stacked through a weak intermolecular interaction, with an interlayer separation of 3.35 Å.[16,17] The structure results in a large anisotropy in thermal properties parallel and perpendicular to the *c*-axis of the crystal.[18−21] Since a defect-free graphite surface shows a minimum tendency toward reactivity and heat conductivity, it is a possible choice for a thermal protection system. It is also a model for ablative material on a spacecraft.[22,23] An interest in gas−surface scattering phenomena associated with graphite results from interpreting microscopic details of the aerodynamic drag of objects with graphitic-like surfaces moving through the atmosphere. N_2 + graphite serves as a prototype model for understanding highly energetic collisions of closed-shell molecules with the surface of spacecraft in low Earth orbit (i.e., at 200−700 km altitude).[24]

Recently, several molecular beam experiments have been performed, wherein a wide range of projectiles (Ar, SF_6, N_2, CO, O_2, Xe) collided with a graphite surface over a range of experimental conditions.[10,25−31] Unlike the experiment for Ar scattering from a graphite surface performed for high-energy collisions,[10] the experimental data for lower-energy collisions

Received: March 16, 2018
Revised: June 14, 2018
Published: June 21, 2018

DOI: 10.1021/acs.jpcc.8b02574
J. Phys. Chem. C 2018, 122, 16048−16059

are quite well described by a simple hard cube model (HCM).[32,33] Oh et al.[28] reported an extensive series of measurements for the angular distribution of O_2 molecules scattered from a graphite surface. Their measurements were carried out over a range of incident energies (291−614 meV) and surface temperatures (150−500 K). They proposed that the gas−surface collision is primarily a single-collision event with large cooperative motions of the carbon atoms in the outermost graphene layer.[28,29]

For the present article, chemical dynamics simulations were performed to investigate energy transfer in collision of O_2 with a graphite (0001) surface. The simulations only consider nonreactive collisions between O_2 and the graphite surface, and possible reactive events are not investigated. The simulations provide an atomic-level understanding of the energy-transfer dynamics and mechanisms for energy transfer to the translational and rotational degrees of freedom of the O_2 projectile. An important component of this study is comparison with experiments by Sibener and co-workers. The simulations follow a recent study of the dynamics of N_2 collisions with a graphite (0001) surface.[34]

II. EXPERIMENTAL APPROACH

The design of the instrument has been previously covered,[35] so only a brief description follows. A molecular beam was produced in the source chamber and passed through several regions of differential pumping before entering an ultra-high-vacuum chamber. The target was mounted on a manipulator that could be rotated with respect to the beam, giving a variable incident (polar) angle, θ_i. The target could be resistively heated to ∼1300 K. A differentially pumped quadrupole mass spectrometer with an acceptance angle of ∼1° could independently rotate around the target so that the final angle (θ_f) was variable. The scattering plane is defined by the arc of this motion.

There were two mechanical choppers, one before and one after the target. The pre-collision chopper had narrow slots for measuring the incident translational energy via time-of-flight. The post-collision chopper had a cross-correlation pattern and was attached to the detector so that it rotated with the mass spectrometer. This was used for all scattering measurements.

The molecular beam was produced by expanding the gas through a small pinhole (15 μm). Varying translational kinetic energies were produced by a combination of heating the nozzle and mixing the O_2 with He. All of the gases used were of UHP grade from Airgas.

The target was highly oriented pyrolytic graphite (SPI, grade 3). Once mounted, the surface of the sample was refreshed by removing the top layers with scotch tape. In vacuum, the sample was also exposed to O_2 at a surface temperature of 1200 K. No attempt was made to align the surface crystallographic directions with the scattering plane. No reaction was observed between O_2 and the surface in the experiments. It may have been occurring, but the rate was too low to observe experimentally.

III. COMPUTATIONAL DETAILS

III.I. O_2 + Graphite Model and Potential Energy Functions. The potential energy function for the O_2 + graphite system is given by

$$V = V_{graphite} + V_{O_2} + V_{O_2+graphite} \quad (1)$$

where $V_{graphite}$ is the graphite potential, V_{O_2} is the O_2 potential, and $V_{O_2+graphite}$ is the O_2 + graphite intermolecular potential.

The graphite model consists of four layers stacked in an AB sequence and is depicted in Figure 1. The carbon atoms in each layer are arranged in a hexagonal pattern forming 15 rings along the x-direction and 12 along the y-direction. The detailed description of the graphite model is given elsewhere,[34] and only salient features of the model are described here. The potential for a graphite layer is represented by C−C harmonic stretches, C−C−C valence angle bends, C−C−C−C dihedral angles, and Lennard-Jones (L-J) (6−12) van der Waals interactions for two C-atoms separated by four or more atoms. Interactions between two C atoms that reside on two adjacent layers are also described by these L-J (6−12) interactions. The parameters for the graphite potential are taken from the all-atom optimized potentials for liquid simulations (OPLS-AA) force field[36] and are given in Table 1 of ref 34. The OPLS scaling of 0.5 is not used for the van der Waals interactions of a 1−4 pair or across the graphene planes. Implementation of a large harmonic force field at the border of the graphite surface, to suppress its distortion, was discussed in detail in our earlier study of N_2 + graphite.[34] For the present study, chemical dynamics simulations of O_2 colliding with graphite are studied at two surface temperatures of 300 and 1177 K. The separations between surface layers at 300 and 1177 K were determined previously as 3.57[34] and 3.62 Å, respectively. The O_2 potential is described by a Morse function with parameters D_e = 220.17 kcal/mol, β_e = 2.78 Å^{-1}, and r_e = 1.2070 Å.[37]

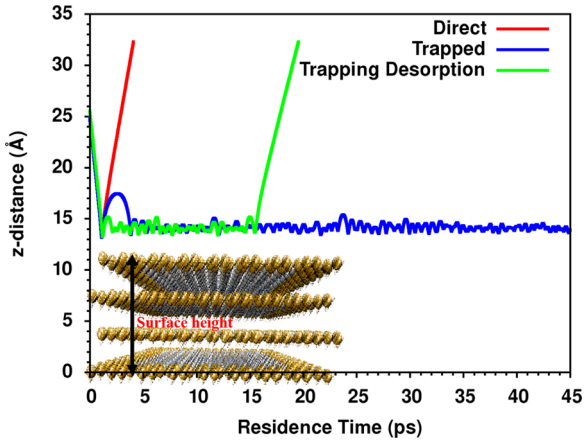

Figure 1. Motion of the O_2 center of mass along the z-direction, i.e., perpendicular to the graphite surface, for the three trajectory types: (1) direct impulsive scattering; (2) trapping desorption or physisorption/desorption; and (3) trapping. R is the z-distance between the center of mass of O_2 and the bottom layer of the graphite surface for the simulation with E_i = 2.1 kcal/mol and θ_i = 45°.

Since benzene is the basic constituent of graphite, an ab initio potential of benzene interacting with O_2 molecule is a quite appropriate choice to mimic the graphite + O_2 interaction. There have been several attempts made to obtain benzene + O_2 interaction energies, but the accuracy of these calculations greatly depends on the electronic structure method.[38,39] Substantial differences are found in the literature for calculations of the interaction energy.[40−44] However, all theoretical calculations establish a common fact that the parallel orientation is the minimal geometry for the benzene−

DOI: 10.1021/acs.jpcc.8b02574
J. Phys. Chem. C 2018, 122, 16048−16059

Table 1. Percentage of Each Trajectory Type[a]

		trajectory types		
T_{surf} (K)	E_i[b]	direct	physisorption/desorption	trapping[c]
300 ± 5	2.1	15 ± 1	15 ± 1 (22)	70 ± 2 (63)
300 ± 5	7.4	46 ± 2	19 ± 1	35 ± 2
301 ± 5	15.0	54 ± 2	19 ± 1	27 ± 2
1177 ± 20	15.0	60 ± 2	40 ± 2	

[a]Incident angle is set to 45° for all simulations. [b]Incident energy given in kcal/mol. [c]O_2 remains trapped on the surface when the trajectory is terminated at 45 ps. The numbers within parentheses are % of trajectory types at the maximum integration time of 75 ps.

O_2 dimer with nearly free rotation of O_2 in the benzene molecular plane. The structure is therefore quite similar to that observed for the benzene−N_2 dimer.[39] In our present study, we used the benzene−O_2 interaction potential proposed by Granucci and Persico.[42] They obtained a value of D_0 = 1.28 kcal/mol (D_e = 1.48 kcal/mol at R_e = 3.36 Å) using SCF/MP2 calculations and corrected to account for the difference between calculated and experimental polarizabilities for both monomers. Their calculated D_0 is only ca. 0.3−0.4 kcal/mol lower than the experimentally reported D_0 value by Grover and co-workers[41] and Casero and Joens.[43,44] The L-J parameters for the O−C interaction, i.e., $V_{O-C} = -\frac{A}{r^m} + \frac{B}{r^n}$, used for current simulations, are A = 486.3 kcal Å^m/mol, B = 506900 kcal Å^n/mol, m = 6, and n = 12.[42]

As discussed above, a four-layer model was used for the graphite surface and, in the previous study of N_2 + graphite scattering,[34] this model gave simulation results in excellent agreement with experiment. In a more recent study of N_2 + graphite scattering,[45] different simulation results were found for graphite models with four and six layers. This surface model used springs with model force constants connecting the layers such that the number of layers changed the surface stiffness. For the current study, the graphene layers of the four-layer surface model interact via L-J (6−12) terms of the OPLS-AA force field[36] and the interaction between two layers is unaffected by other layers. The stiffness of the top layer, next layer, etc. is unaffected by the presence of underlying layers. In a recent simulation study of Ar + graphite hyperthermal scattering,[10] the scattering dynamics was found to be the same for model surfaces with two and three layers.

III.II. Procedure for the Chemical Dynamics Simulations. Classical trajectories were used to simulate collisions of a beam of O_2 molecules with the graphite (0001) surface. The trajectory simulations were performed with the general chemical dynamics computer program VENUS.[46,47] Initial conditions for the trajectories were chosen to model experiments by Sibener and co-workers. Collisions between O_2 and graphite were simulated for three incident beam translational energies E_i of 2.1, 7.4, and 15.0 kcal/mol. The incident angle θ_i, defined by the angle between the O_2 initial velocity vector and the surface normal, was set to 45° for all of the trajectories. Chemical dynamics simulations for each E_i were carried out at surface temperature T_{surf} = 300 K. For the higher surface temperature of 1177 K, a simulation was only performed for E_i = 15 kcal/mol.

Sampling of initial conditions follows our previous N_2 + graphite simulations.[34] For each simulation, a beam of colliding O_2 molecules was randomly aimed within a circular area of radius 2.2 Å so that the area spanned by the O_2 beam covered a hexagonal unit cell on the graphite surface. O_2 was randomly rotated about its Euler angles. Each trajectory was initiated with a separation of 20 Å between the center of the beam and the surface aiming point. The projection of the O_2 beam onto the graphite surface is defined by an azimuthal angle (χ_f) and chosen randomly between 0 and 360°. The initial ro-vibrational quantum states of the O_2 molecules were sampled from a 300 K Boltzmann distribution for E_i = 2.1 and 7.4 kcal/mol and from a 500 K distribution for E_i = 15.0 kcal/mol. These are the temperatures of the nozzle in the molecular beam experiments conducted by Sibener et al. The O_2 rotational angular momentum j was related to the O_2 rotational quantum number J via $j = \sqrt{[J(J+1)]}\hbar$. Einstein−Brillouin−Keller (EBK) semiclassical quantization[48] was used to add the O_2 vibrational quantum number n. The O_2 internal energy is given by

$$E = p^2/2\mu + V(r) + j^2/2\mu r^2 \quad (2)$$

This sampling includes O_2 zero-point energy.

Periodic boundary conditions were employed along the x- and y-directions of the graphite surface. The x, y, and z dimensions of the primary box are 29.5, 32.6, and 10.5 Å, respectively. For each trajectory, the bottom layer of the graphite surface was held rigid and acted as an anchor layer. Initial conditions for the graphite surface were selected by assigning velocities to the carbon atoms of the first, second, and third layers, sampled from a Maxwell−Boltzmann distribution at a given surface temperature. The surface was then equilibrated by a 50 or 75 ps molecular dynamics simulation for surface temperatures of 300 or 1177 K, respectively, with velocity rescaling every 5 fs. This is followed by a 50 or 80 ps equilibration, without velocity rescaling. The average surface temperature attained after the equilibration is 300 or 1177 K, respectively.

The trajectories were propagated with a combined fourth-order Runge−Kutta and sixth-order Adams−Moulton algorithm, with a time step of 0.05 fs. Trajectories were terminated by either a distance criterion, i.e., when the distance between the aiming point and the outgoing O_2 distance exceeds 30 Å, or a total integration time criterion, i.e., the total integration time exceeds 45 ps. The latter is used for trapped trajectories with O_2 remaining on the surface, for the simulations with E_i of 7.4 and 15 kcal/mol. For the lowest-energy simulations with E_i = 2.1 kcal/mol, the maximum integration time was set to 75 ps. Typically, 800 trajectories were calculated for each ensemble of initial conditions (E_i, θ_i, T_{surf}). Energy conservation was within 1% for each trajectory.

At the end of each trajectory, the final translational and internal energies of the O_2 molecule and the internal energy of the surface are evaluated. The O_2 rotational quantum number is calculated from its final rotational angular momentum, and the Einstein−Brillouin−Keller (EBK) semiclassical quantization[48] is used to find the O_2 vibrational quantum number. The final angular distribution $P(\theta_f)$ of the scattered O_2 molecule is

DOI: 10.1021/acs.jpcc.8b02574
J. Phys. Chem. C 2018, 122, 16048−16059

determined by calculating the angle between the final velocity vector of the projectile and the surface normal. The distribution of the final azimuthal angle, with respect to the scattering plane, $P(\chi_f)$ is also calculated. Statistical uncertainties were calculated for the simulation results. The uncertainty in a component of a distribution is the standard deviation. The uncertainty in an average value is the standard deviation of the mean.

IV. RESULTS AND DISCUSSION

IV.I. O_2 + Graphite Atomistic Collision Dynamics: Inner Turning Point (ITP) and Residence Time. To classify the trajectory type, the number of inner turning points (ITPs) was counted for each trajectory. From this analysis, three types of trajectory were identified: direct (single ITP), physisorption/desorption with multiple ITPs (MITPs), and trapping on the surface with MITPs, with O_2 remaining on the surface when the trajectory was terminated. Representative trajectories of each trajectory type are demonstrated in Figure 1, by showing the z-coordinate of O_2 with respect to the graphite rigid layer versus time. There were no trajectories found for which O_2 penetrated the top graphite layer, the same behavior observed in N_2 + graphite collisions.[35] Trajectories for which O_2 remained trapped on the surface, when the trajectories were halted, are excluded from analyses of E_f, θ_f, and χ_f.

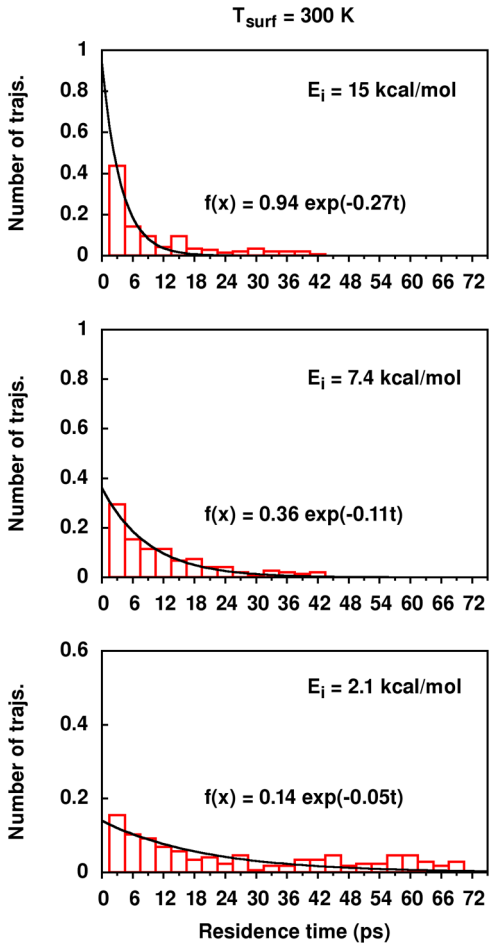

Figure 2. Distribution of the residence time for physisorption/desorption trajectories.

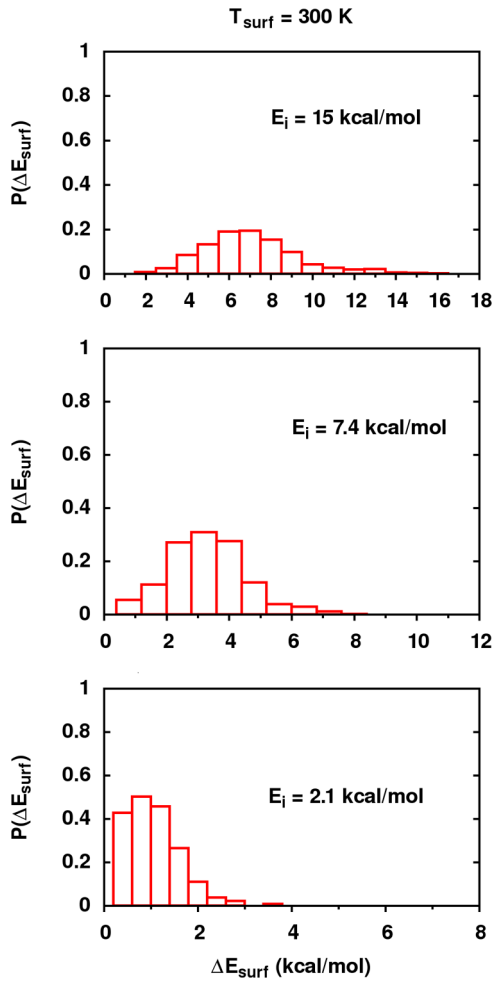

Figure 3. Distributions of ΔE_{surf}, $P(\Delta E_{surf})$, for T_{surf} = 300 K and θ_i = 45° with different E_i values.

Table 1 presents percentages of the three trajectory types as a function of incident energy and surface temperature. In our

Table 2. Percentage of Average Energies Transferred for Different Trajectory Types

		trajectory type								
		direct scattering			physisorption/desorption			total		
T_{surf}	E_i[b]	$\langle E_f \rangle$	$\langle \Delta E_{surf} \rangle$	$\langle \Delta E_{int} \rangle$[a]	$\langle E_f \rangle$	$\langle \Delta E_{surf} \rangle$	$\langle \Delta E_{int} \rangle$	$\langle E_f \rangle$	$\langle \Delta E_{surf} \rangle$	$\langle \Delta E_{int} \rangle$
300	2.1	77	22	1	68	28	4	71	26	3
	7.4	63	35	2	46	51	3	58	40	2
	15.0	58	40	2	42	57	1	54	44	2
1177	15.0	58	35	7	66	25	9	62	31	7

[a]The percentage for ΔE_{int} is equivalent to ΔE_{rot}, since ΔE_{vib} = 0 for all trajectories. [b]Energy in kcal/mol.

DOI: 10.1021/acs.jpcc.8b02574
J. Phys. Chem. C 2018, 122, 16048−16059

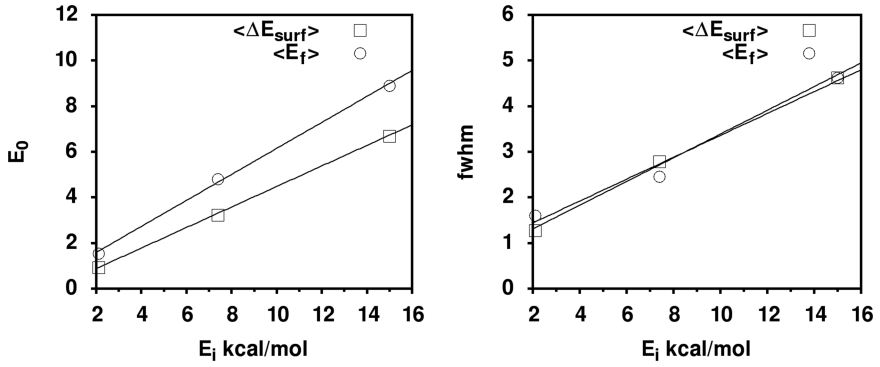

Figure 4. Plots of fwhm and energy center E_o, for each $P(E_{surf})$, versus E_i; with fits to eq 3.

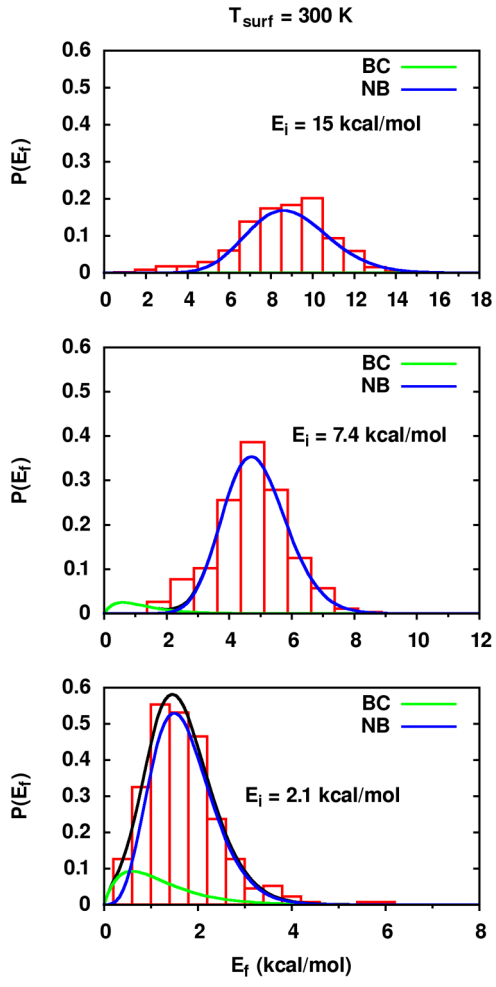

Figure 5. Distributions of E_f, $P(E_f)$, for T_{surf} = 300 K and θ_i = 45° with different E_i values. The fits include Boltzmann and non-Boltzmann components, i.e., BC and NB.

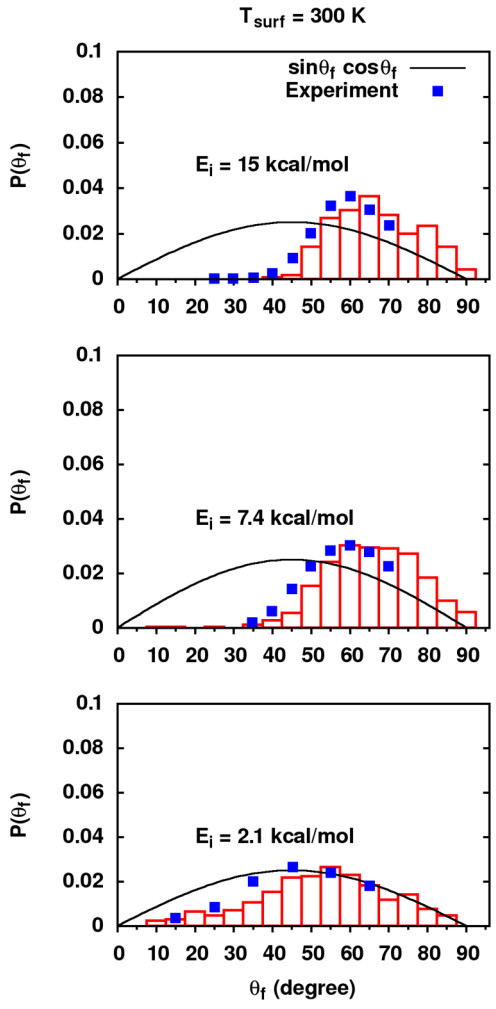

Figure 6. Angular distributions of θ_f, $P(\theta_f)$, for E_i = 2.1, 7.4, and 15 kcal/mol; T_{surf} = 300 K and θ_i = 45°. The solid line is the random distribution. $P(\theta_f)$ is for all azimuthal angles and not just in-plane scattering. The square symbol represents the experimental angular distributions.

previous study of N_2 + graphite,[34] we found that at smaller incident angles with respect to the surface normal, the molecule−surface collisions are dominated by direct scattering, while physisorption/desorption becomes important at higher incident angles. In the present study, we have fixed the incident angle at 45° to compare with experiment. As shown in Table 1, with increase in E_i, the direct scattering percentage increases to 15, 46, and 54% for E_i = 2.1, 7.4, and 15 kcal/mol, respectively, for the surface temperature of 300 K.

For the E_i = 15 kcal/mol simulations and T_{surf} = 300 K, O_2 interacts with the surface for a longer time than for the simulations with T_{surf} = 1177 K. For the latter T_{surf}, there are no O_2 molecules adsorbed/trapped on the surface when the trajectories are terminated at 45 ps. Less trapping on the surface is expected for the higher T_{surf}. For the simulations with E_i of 2.1 kcal/mol, 70 and 63% of the O_2 molecules remained trapped on the surface for trajectory integration times of 45

DOI: 10.1021/acs.jpcc.8b02574
J. Phys. Chem. C 2018, 122, 16048−16059

Table 3. Average Scattering Angles for Different Trajectory Types for the Surface Temperature of 300 K

	trajectory type		
E_i	direct $\langle\theta_f\rangle$	physisorption/desorption $\langle\theta_f\rangle$	total $\langle\theta_f\rangle$
2.1	56	46	50
7.4	63	63	63
15.0	63	69	64

and 75 ps, respectively. If the trajectories were integrated for a longer period of time, a smaller percentage of O_2 would have remained trapped. At long time, it is expected that all of the O_2 will desorb. Similarly, for the simulations with E_i of 7.4 and 15 kcal/mol and T_{surf} = 300 K, all of the trapped trajectories are expected to ultimately desorb. In Figure 2, histograms are given for the distribution of residence times for the physisorption/desorption trajectories. For E_i of 15 and 7.4 kcal/mol, a significant fraction of the O_2 molecules leaves the surface within 1−3 ps. However, for the lowest incident energy, a long tail extending to longer residence times is observed. The physisorption/desorption residence time distribution decreases exponentially, with an increase in average residence time with decrease in E_i. The rate at which the distribution decreases shows a near-linear dependence with E_i.

In previous chemical dynamics simulations of N_2 collisions with the graphite surface,[34,45] the three trajectory types of direct scattering, physisorption/desorption, and trapping were observed, as found here for O_2 + graphite scattering. In contrast, analyses with the hard cube and smooth surface theoretical models indicate that the dynamics is dominated by direct scattering.[28,29] The atomistic chemical dynamics with potential energy surfaces results in dynamics different from that predicted by the theoretical models.

Trampoline-like undulations of the graphite surface were observed in simulations of the massive Xe-atom colliding with the graphite surface.[30] Such undulations were not seen in the current simulations of the lighter O_2 molecule colliding with graphite.

IV.II. Energy-Transfer Efficiency. During the O_2 collision with the graphite surface, part of E_i of O_2 is transferred to its internal vibrational/rotational degrees of freedom (E_{int}) and surface vibration energy (E_{surf})

$$E_i = \Delta E_{int} + \Delta E_{surf} + E_f \quad (3)$$

where E_f is the O_2 final translation energy. The values of ΔE_{int}, ΔE_{surf}, and E_f are determined upon completion of each trajectory. This information is then presented as a histogram to determine the distribution of each energy term.

In Table 2, the average percentage energies transferred to $\langle\Delta E_{int}\rangle$, $\langle\Delta E_{surf}\rangle$, and $\langle E_f\rangle$ are presented for the 300 K surface temperature simulations with E_i = 2.1, 7.4, and 15 kcal/mol, respectively. There are no restrictions on the final scattering angles θ_f and χ_f. A negligible percentage of E_i is transferred to the O_2 rotation, with no transfer to vibration. Transfer to O_2 rotation is independent of E_i, with average energy-transfer

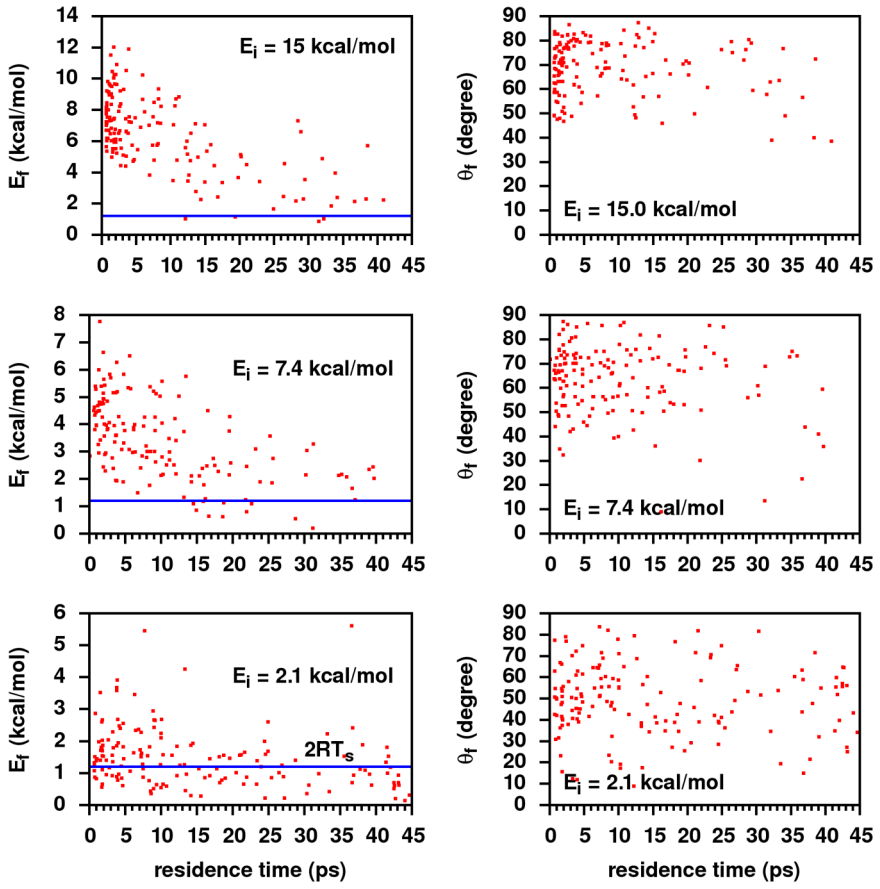

Figure 7. Scatter plots of E_f and θ_f versus residence time for physisorption/desorption trajectories, with E_i = 2.1, 7.4, and 15 kcal/mol. For these simulations, θ_i is fixed at 45° and T_{surf} = 300 K. The solid line corresponds to the translational energy of $2RT_{surf}$.

DOI: 10.1021/acs.jpcc.8b02574
J. Phys. Chem. C 2018, 122, 16048−16059

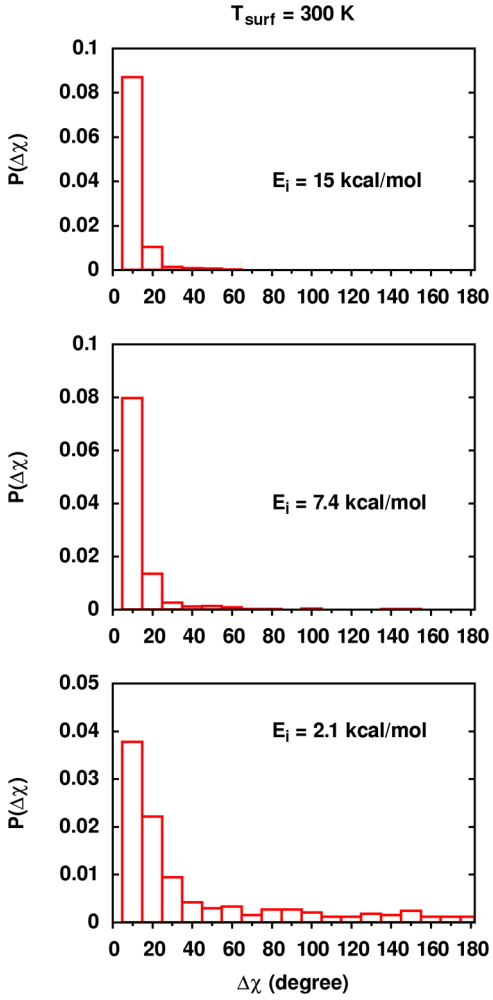

Figure 8. Distributions of the change in the azimuthal angle $\Delta\chi_f = \chi_f - \chi_i$; $\theta_i = 45°$.

percentages of 1−2%. Therefore, the loss of E_i is primarily to the surface, with percentages of 26, 40, and 44% for E_i of 2.1, 7.4, and 15 kcal/mol, respectively, for the total trajectories. Simultaneously, the percentages of the average energy remaining in O_2 translation are 71, 58, and 54%, respectively. The increase in surface vibration with an increase in incident energy was also observed for N_2 + graphite[34] and CO_2 + F-self-assembled monolayer (SAM) collisions.[49] For the ensemble (E_i, T_{surf}) = (15, 1177), 62% of E_i remained in O_2 translation with a 31% loss to the surface. For the above simulation, with the same E_i but T_{surf} = 300 K, the transfer to the surface is 44%.

A separate analysis is done for each trajectory type, and the percentages of the average energy transferred are listed in Table 2. It is evident from the analysis that physisorption/desorption plays a major role in energy transfer to the surface. The percentage transfers to $\langle\Delta E_{surf}\rangle$ for direct scattering are 22, 35, and 40%, whereas for physisorption/desorption, the values are 28, 51, and 57% for E_i = 2.1, 7.4, and 15 kcal/mol, respectively. The distributions of $P(\Delta E_{surf})$ for the 300 K simulations are given in Figure 3, and all three are quite well described by a Gaussian distribution.

$$f(E) = A\, e^{(E-E_0)^2/2\sigma^2} \tag{4}$$

The full width at half-maximum (fwhm) and energy center (E_o) are determined for each distribution, and their variations with E_i are depicted in Figure 4. A linear regression analysis clearly displays that both parameters are a linear function of the incident energy. This analysis helps to predict the energy distribution at any given E_i. A similar relationship was also found for N-protonated octaglycine collisions with an H-SAM surface.[50] The physical significance of this linear relationship has not been established.

The probability distribution of the final O_2 translational energy is given in Figure 5. The extent of thermalization is determined by the fraction of $P(E_f)$ described by the Boltzmann energy distribution. The value of f_{BC} is determined by nonlinear least-squares fitting of the total distribution $P(E_f)$, given by

$$P(E_f) = f_{NB}A^{-1}E_f \exp\left\{-\frac{m\left[\left(\frac{2E_f}{m}\right)^{1/2} - \nu_2\right]^2}{2k_BT_2}\right\} + f_{BC} (k_BT_{surf})^2\, E_f \exp\left(-\frac{E_f}{k_BT_{surf}}\right) \tag{5}$$

where f_{NB} is the non-Boltzmann component and $f_{BC} + f_{NB} = 1$. The temperature of the Boltzmann component is fixed at the surface temperature. The fitting parameters are f_{BC}, T_2, ν_2, and A. Equation 5 was used previously to analyze $P(E_f)$ for Ne + squalane and Ar + H-SAM and HO-SAM scattering.[51,52] Figure 5 clearly depicts that $P(E_f)$ is mainly dominated by the NB component, and its contributions are 0.85, 0.96, and 1.00 for E_i = 2.1, 7.4, and 15 kcal/mol, respectively. The fwhm and E_f^{max} obtained from each distribution by fitting to a Gaussian distribution are plotted against E_i in Figure 4. Like $\langle\Delta E_{surf}\rangle$, $\langle E_f\rangle$ also shows a strong linear dependence with E_i.

As found for our previous N_2 + graphite simulation,[34] there is no surface site dependence for the O_2 + graphite scattering dynamics. Energy transfer upon impact with the surface determines whether O_2 will directly scatter or physisorb with MITPs. This energy transfer is strongly influenced by the short-range repulsion of the O_2-graphite potential and expected to be also affected by the orientation of O_2 during the collision. Energy dissipation within the surface after O_2 impact is an interesting question, but was not investigated in the current study.

In the simplest models of energy transfer in gas−surface collisions, it is only the normal component E_i^n of E_i which participates in energy transfer and the parallel component is conserved. For the current simulations with θ_i = 45° and for the direct scattering trajectories, a linear relationship was found between the normal component of incident energy $E_i^n = E_i \cos^2\theta_i = E_i/2$ and the energy transferred ($E_i - E_f$) to the surface. For E_i = 7.4 and 15 kcal/mol, 37 and 42% of energy were transferred, respectively. These percentages are similar to those reported using the hard cube model (HCM) for O_2 + graphite energy transfer.[28] For T_{surf} = 500 K and E_i from 6.7 to 14 kcal/mol, the HCM percentage energy transfer increased from 30 to 38%. For $E_i \sim 6$ kcal/mol and T_{surf} = 300 K, the energy transfer is 36%. In our previous study of N_2 + graphite collisions,[34] we obtained an energy loss of ∼29%, which matched quite well with the estimated value for the HCM of ∼27%.

IV.III. Scattering and Azimuthal Angle Distributions.

The angular distribution $P(\theta_f)$ of scattered O_2 for all azimuthal directions is shown in Figure 6 for E_i of 2.1, 7.4, and 15 kcal/

DOI: 10.1021/acs.jpcc.8b02574
J. Phys. Chem. C 2018, 122, 16048−16059

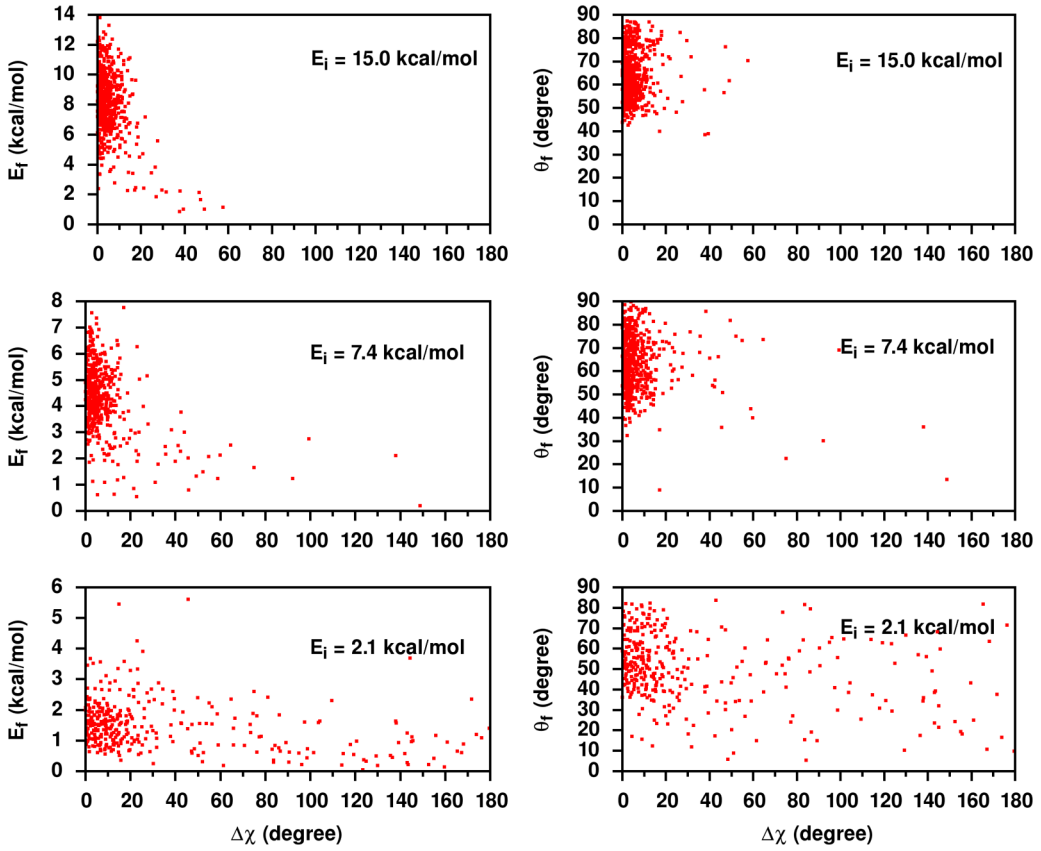

Figure 9. Scatter plots of E_f and θ_f versus change in the azimuthal angle $\Delta\chi$, with E_i = 2.1, 7.4, and 15 kcal/mol. For these simulations, θ_i is fixed at 45° and T_{surf} = 300 K.

mol. For random scattering, $P(\theta_f)$ follows $\sin(\theta)\cos(\theta)$, and these dynamics are approximately observed for the lowest E_i, but scattering with $\theta_f > 45°$ is more pronounced than for $\theta_f < 45°$. However, with increasing incident energy, the behavior starts to substantially deviate from this distribution, and the maximum θ_f^{max} in the angular intensity distribution appears at an angle much larger than the specular angle $\theta_f = \theta_i$. This implies that during the collision, the particle has lost energy to the surface, which is consistent with the dominance of direct scattering for the larger E_i and transfer of a fraction of the normal component of E_i to the surface. For low-incident-energy collisions with E_i = 2.1 kcal/mol, the angular deviation from the lobular maximum in the specular direction is only 5°, but for higher-energy collisions, the deviation becomes larger, and for E_i of 7.4 and 15.0 kcal/mol, the deviations are ∼18 and 19°, respectively (see Figure 6). The distributions $P(\theta_f)$, shown in Figure 6, are for all scattering trajectories including both in and out of plane. The distributions are not divided by $\sin\theta_f$.

To understand the contribution of each trajectory type to the angular distribution, listed in Table 3 are the average final scattering angles $\langle\theta_f\rangle$ for the different trajectory types. Interestingly, $\langle\theta_f\rangle$ for physisorption/desorption at high collision energies shows a significant deviation from 45° and instead has a value for a supraspecular angle. In our earlier study of N_2 + graphite collisions,[34] a similar behavior was observed and the trapping was categorized as quasi-trapping.[53] Unlike conventional trapping, quasi-trapping involves very rapid equilibration of the normal component of E_i but very slow accommodation of the parallel component. Therefore, for higher surface temperatures when the residence time of projectile is very short, the projectile desorbs from the surface before it is fully thermalized, resulting in memory of the parallel component.

To further confirm whether the present system exhibits quasi-trapping, the final scattered angle θ_f and energy E_f are plotted in Figure 7 as a function of residence time for desorbing trajectories with E_i = 2.1, 7.4, and 15.0 kcal/mol. For thermal desorption and full equilibration, $\langle E_f\rangle$ is $2RT_s$ and $\langle\theta_f\rangle$ is 45°. As depicted in Figure 7, for higher-energy collisions, most of the desorbing trajectories leave the surface after a short residence time of 5−10 ps, with a translational energy greater than $2RT_s$ and not fully thermalized with the surface. Longer residence times are more important for the low-energy E_i = 2.1 kcal/mol collisions, and for times of ∼10 ps and greater, desorption follows the conventional definition of physisorption/desorption with both the parallel and normal momenta of O_2 fully equilibrated and O_2 scattered randomly.

Distribution of the change in the azimuthal angle $\Delta\chi_f = \chi_f - \chi_i$ is plotted in Figure 8. For E_i = 7.4 and 15.0 kcal/mol, with only 19% physisorption/desorption, the $\Delta\chi$ distribution is strongly peaked at 0 ± 10°, whereas for E_i = 2.1 kcal/mol, for which physisorption/desorption dominates, the $\Delta\chi$ distribution is expected to be more uniform with the same probability at every final azimuthal angle. However, as shown in Figure 8, the population is not completely uniform, since populations of smaller values of $\Delta\chi$ are higher compared to those of larger values. Only including desorbing trajectories with a residence time greater than ∼10 ps results in a more uniform probability for the azimuthal angle, and the uniformity increases with increase in residence time. The scatter plots of both E_f and θ_f

DOI: 10.1021/acs.jpcc.8b02574
J. Phys. Chem. C 2018, 122, 16048−16059

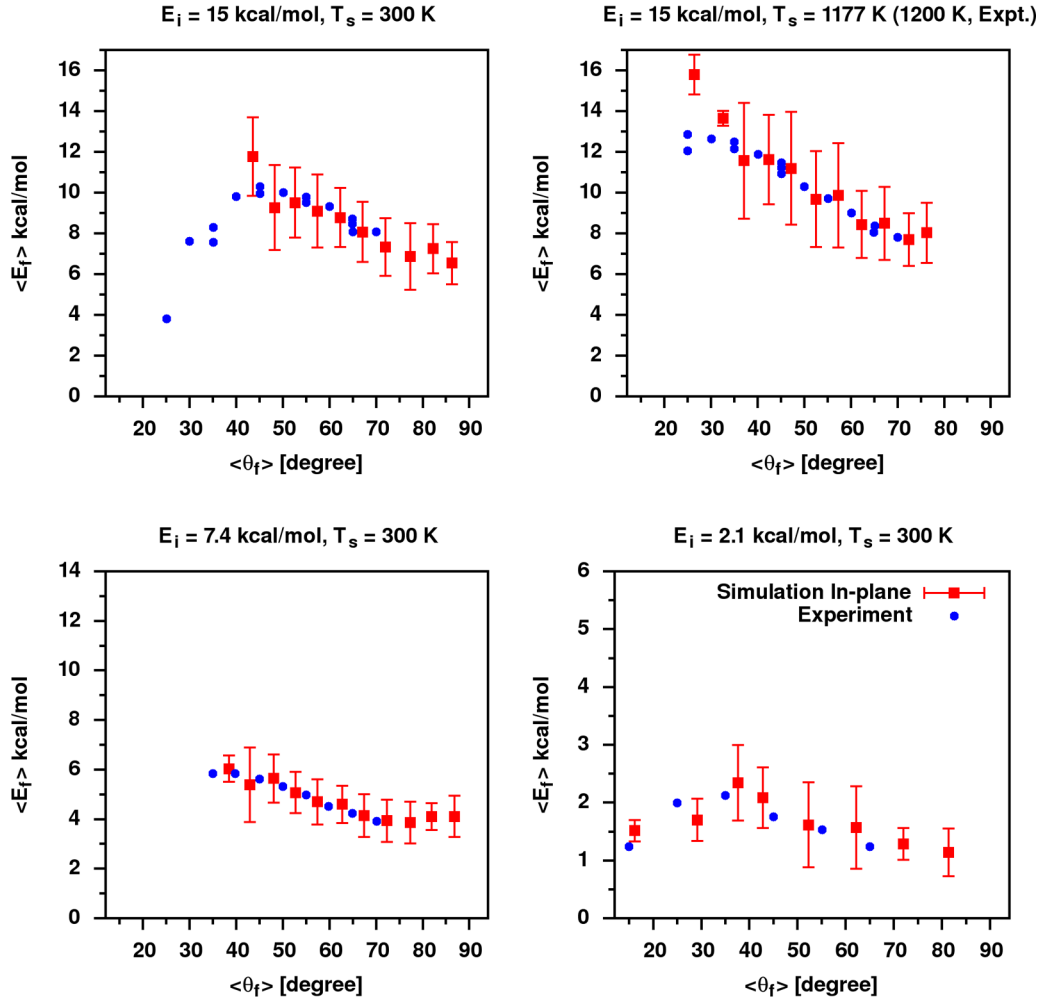

Figure 10. Plots of $\langle E_f \rangle$ versus $\langle \langle \theta_f \rangle \rangle$ for the four ensembles E_i (kcal/mol), T_{surf} (K) = (2.1, 300), (7.4, 300), (15, 300), and (15, 1177). For higher surface temperature, the experiment was carried out at 1200 K. Included are comparisons with experiment.

versus $\Delta\chi$ are given in Figure 9. The clustering of points in the region of 0 ± 10° for the higher-energy collisions clearly depicts that the scattering primarily remains in the incident plane and for each θ_f retention of a relatively large fraction of the incident collision energy in the final translation. It is worth mentioning that even though the highest incident energy considered here is larger than $2RT_s$, it is not sufficient to cross the threshold for a transformation in the scattering from the thermal to the structural regime.[5,54]

IV.IV. Comparison between Simulations and Experiments. Sibener and co-workers measured properties associated with the dynamics of O_2 scattering off graphite in the incident plane at E_i = 2.1, 7.4, and 15.0 kcal/mol, θ_i = 45°, with surface temperatures of 300 and 1200 K. In the experiments, all measurements were restricted to θ_f = 20−70°. For a direct comparison with experiment, it is essential to obtain simulation results for in-plane scattering and, therefore, to accomplish this, the simulation results for $\|\Delta\chi\| \leq 10°$ were used to approximate in-plane scattering.[8,51,55,56] This approximation is quite acceptable; as shown in Figure 8 for high-energy collisions, there is a clustering of points in the $\Delta\chi$ region of 0 ± 10°. For the three E_i = 2.1, 7.4, and 15.0 kcal/mol, at 300 K, the respective percentages of trajectories that scattered within ± 10° of the scattering plane are 38, 80, and 87%. The average final translational energy of scattered O_2 molecules as a function of the final scattering angle θ_f is presented in Figure 10, for both simulations and experiments. The agreement between simulation and experiment is excellent. The probability distributions of the final translational energy for in-plane scattering obtained from the simulations are compared to the experimental $P(E_f)$ distributions in Figure 11. It should be noted that for the experimental distributions, θ_f = 50°; however, for the simulations, no such restriction was made and all θ_f are included. The average θ_f values for the simulations, $\langle \theta_f \rangle$, are given in the figure.

The experimental and simulation angular distributions of θ_f, $P(\theta_f)$, are compared in Figure 6, and there is excellent agreement. However, it should be noted that the experimental distribution is for in-plane scattering, while that for the simulations includes all azimuthal directions.

When the T_{surf} = 300 K simulations were terminated, some of the O_2 molecules remained trapped on the graphite surface. These molecules are expected to be thermally accommodated with the surface and thus desorb randomly in the 0−2π final azimuthal angles χ_f. As a result, this scattering will contribute a negligibly small addition to the short time scattering, which is in (or near) the scattering plane, defined by the detector and the O_2 molecular beam. They will not affect comparison with the experimental in-plane scattering.

DOI: 10.1021/acs.jpcc.8b02574
J. Phys. Chem. C 2018, 122, 16048−16059

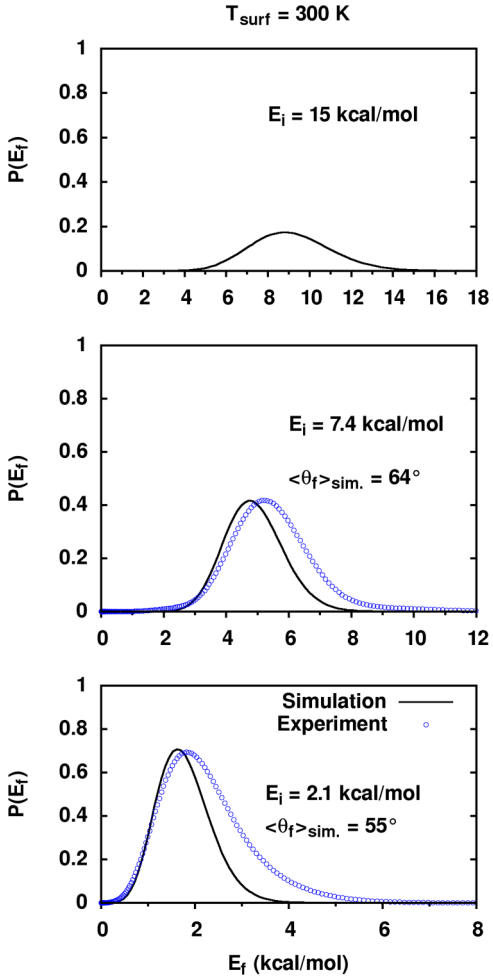

Figure 11. Comparison between experimental and simulation $P(E_f)$ distributions of the final translational energy for in-plane scattering; θ_i = 45° and θ_f fixed at 50° for the experiments.

V. CONCLUSIONS

In this study, chemical dynamics simulations were performed to study O_2 + graphite gas−surface scattering. The simulations were performed for three collision energies E_i of 2.1, 7.4, and 15 kcal/mol, with the initial incident angle fixed at θ_i = 45°. O_2 scattering from graphite shows scattering dynamics similar to that observed previously in N_2 + graphite scattering.[34] The simulations only considered nonreactive collisions between O_2 and the graphite surface, and possible reactive events were not investigated. The following are the important scattering dynamics determined from the simulations:

(1) For larger E_i values of 15 and 7.4 kcal/mol, a significant fraction of the O_2 molecules scatter from the surface in 1−3 ps. However, for the lowest incident energy, there is a long tail extending to much longer residence times. The trapping desorption residence time distribution follows an exponential decay with an increase in residence time with decrease in E_i. The rate at which the distribution decreases shows a near-linear dependence with increase in incident energy.

(2) The average energy transferred to the surface and that remaining in O_2 translation, i.e., $\langle \Delta E_{surf} \rangle$ and $\langle E_f \rangle$, also show a strong linear dependence with initial translational energy, illustrating that their energy distributions may be predicted for any initial collisional energy.

(3) Scattering for all incident angles is dominated by near in-plane scattering, with non-in-plane scattering becoming important for the low E_i of 2.1 kcal/mol and long residence times. For higher collision energies E_i of 7.4 and 15 kcal/mol, the angular distribution of the scattered O_2 is nonrandom, with a single peak at an angle close to the specular angle. For these collision energies, most of the desorbing trajectories leave the surface after a short residence time with a translational energy greater than the $2RT_s$ value for full thermal equilibration with the surface. Low-energy (2.1 kcal/mol) collisions of O_2 with graphite, for residence times of ∼10 ps and longer, follow conventional trapping desorption with both the parallel and normal momenta of the projectile fully equilibrated and the projectile scattered in random directions.

(4) For all of the scattering conditions considered experimentally, the relationship between the average final translational energy and average scattering angle for the O_2 molecules found from the simulations is in excellent agreement with the experimental results obtained by Sibener and co-workers.

An interesting question is whether the initial energy transfer to the graphite surface is to the interplane or intraplane motions. However, because of anharmonic couplings between these motions, e.g., out-of-plane intraplane and interplane motions, an unambiguous answer is not possible. Such couplings were observed in a simulation of Ne-atom collisions with an alkylthiolate self-assembled monolayer (H-SAM) surface.[55] During a collision, intramolecular vibrational energy redistribution occurred between low-frequency modes of H-SAM chains and chain−chain intermolecular motions. Mode-specific energy transfer to the graphite surface may be studied using a normal mode Hamiltonian for the surface,[57] and such simulations may be pursued in future research.

Finally, it would be of interest to study the O_2 + graphite energy-transfer dynamics, as well as those for N_2 + graphite,[34] as a function of the projectile's orientation as it collides with the surface. In the current study for O_2 and in the previous study for N_2,[34] the orientation of the projectile is chosen randomly with a thermal rotational energy and it was not possible to study these orientation dynamics. In future simulations, it would be of interest to fix the initial orientation of the O_2/N_2 projectile, without rotation excitation, and investigate how the energy-transfer dynamics is affected by the projectile's orientation.[58]

AUTHOR INFORMATION

Corresponding Author

*E-mail: bill.hase@ttu.edu.

ORCID

Moumita Majumder: 0000-0003-3928-957X
S. J. Sibener: 0000-0002-5298-5484
William L. Hase: 0000-0002-0560-5100

Notes

The authors declare no competing financial interest.

ACKNOWLEDGMENTS

The research reported here is based on work supported by the Air Force Office of Scientific Research grant FA9550-16-1-0133 and the Robert A. Welch Foundation grant D-0005. Support was also provided by the High Performance

DOI: 10.1021/acs.jpcc.8b02574
J. Phys. Chem. C 2018, 122, 16048−16059

Computing Center at Texas Tech University under the direction of Alan Sill. Some of the computations were also performed on the Chemdynm cluster of the Hase Research Group. S.J.S. acknowledges the support from the Air Force Office of Scientific Research grant FA9550-15-1-0428, as well as support from the NSF-Materials Research Science and Engineering Center at The University of Chicago (Grant no. NSF-DMR-14-20709).

REFERENCES

(1) Rettner, C. T.; Auerbach, D. J.; Tully, J. C.; Kleyn, A. W. Chemical Dynamics at the Gas-Surface Interface. *J. Phys. Chem.* **1996**, *100*, 13021−13033.
(2) Nogueira, J. J.; Hase, W. L.; Martinez-Nunez, E. Understanding Energy Transfer in Gas-Surface Collisions from Gas-Phase Models. *J. Phys. Chem. C* **2014**, *118*, 2609−2621.
(3) Bosio, S. B. M.; Hase, W. L. Energy Transfer in Rare Gas Collisions with Self-Assembled Monolayers. *J. Chem. Phys.* **1997**, *107*, 9677−9686.
(4) Barnes, G. L.; Hase, W. L. Energy Transfer, Unfolding, and Fragmentation Dynamics in Collisions of N-Protonated Octaglycine with an H-SAM Surface. *J. Am. Chem. Soc.* **2009**, *131*, 17185−17193.
(5) Goodman, F. O.; Wachman, H. Y. *Dynamics of Gas-Surface Scattering*; Academic Press: New York, 1976.
(6) Yan, T.; Hase, W. L. Origin of the Boltzmann Translational Energy Distribution in the Scattering of Hyperthermal Ne atoms off a Self-Assembled Monolayer. *Phys. Chem. Chem. Phys.* **2000**, *2*, 901−900.
(7) Martínez-Núñez, E.; Rahaman, A.; Hase, W. L. Chemical Dynamics Simulations of CO_2 Scattering on a Fluorinated Self-Assembled Monolayer Surface. *J. Phys. Chem. C* **2007**, *111*, 354−364.
(8) Tasić, U. S.; Tan, T.; Hase, W. L. Dynamics of Energy Transfer in Collisions of $O(^3P)$ atoms with a 1-Decanethiol self-Assembled Monolayer Structure. *J. Phys. Chem. B* **2006**, *110*, 11863−11877.
(9) Yamanishi, N.; Matsumoto, Y.; Shobatake, K. Multistage Gas-Surface Interaction Model for the Direct Simulation Monte Carlo Method. *Phys. Fluids* **1999**, *11*, 3540−3552.
(10) Gibson, K. D.; Sibener, S. J.; Upadhaya, H. P.; Brunsvold, A. L.; Zhang, J.; Minton, T. K.; Troya, D. Hyperthermal Ar Atom Scattering from C(0001) Surface. *J. Chem. Phys.* **2008**, *128*, No. 224708.
(11) Mehta, N. A.; Levin, D. A.; Murray, V. J.; Minton, T. K. Study of Non-Reactive Scattering from Graphene using Molecular Beam Experiments and Molecular Dynamics. *AIP Conf. Proc.* **2016**, *1786*, No. 100003.
(12) Morón, V.; Martin-Gondre, L.; Gamallio, P.; Sayós, R. Dynamics of the Oxygen Molecules Scattered from the Graphite (0001) Surface and Comparison with Experimental Data. *J. Phys. Chem. C* **2012**, *116*, 21482−21488.
(13) Lu, J. W.; Day, B. S.; Fiegland, L. R.; Davis, E. D.; Alexander, W. A.; Troya, D.; Morris, J. R. Interfacial Energy Exchange and Reaction Dynamics in Collisions of Gases on Model Organic Surfaces. *Prog. Surf. Sci.* **2012**, *87*, 221−252 and references therein..
(14) Sitz, G. O.; Kummel, A. C.; Zare, R. N.; Tully, J. C. Direct Inelastic Scattering of N_2 from Ag (111). II. Orientation. *J. Chem. Phys.* **1988**, *89*, 2572−2582.
(15) Ueta, H.; Gleeson, M. A.; Kleyn, A. W. The Interaction of Hyperthermal Nitrogen with N-Covered Ag (111). *J. Chem. Phys.* **2011**, *135*, No. 074702.
(16) Pierson, H. O. *Handbook of Carbon, Graphite, Diamond and Fullerenes*; Noyes Publications, 1993.
(17) Chung, D. D. L. Review Graphite. *J. Mater. Sci.* **2002**, *37*, 1475−1489.
(18) Slack, G. A. Anisotropic Thermal Conductivity of Pyrolytic Graphite. *Phys. Rev.* **1962**, *127*, 694−701.
(19) Klemens, P. G.; Pedraza, D. F. Thermal Conductivity of Graphite in the Basal Plane. *Carbon* **1994**, *32*, 735−741.
(20) Sun, K.; Stroscio, M. A.; Dutta, M. Graphite C-axis Thermal Conductivity. *Superlattices Microstruct.* **2009**, *45*, 60−64.
(21) Harb, M.; Schmising, C. v. K.; Enguist, H.; Jurgilaitis, A.; Maximov, I.; Shvets, P. V.; Obraztsov, A. N.; Khakhulin, D.; Wulff, M.; Larsson, J. The C-Axis Thermal Conductivity of Graphite film of Nanometer Thickness Measured by Time Resolved X-Ray Diffraction. *Appl. Phys. Lett.* **2012**, *101*, No. 233108.
(22) Lachaud, J.; Cozmuta, I.; Mansour, N. N. Multiscale Approach to Ablation Modeling of Phenolic Impregnated Carbon Ablators. *J. Spacecr. Rockets* **2010**, *47*, 910−921.
(23) Desai, T. G.; Lawson, J. W.; Keblinski, P. Modeling Initial Stage pf Phenolic Pyrolysis: Graphite Precursor formation and Interfacial Effects. *Polymer* **2011**, *52*, 577−585.
(24) Murad, E. Spacecraft Interaction with Atmospheric Species in Low Earth Orbit. *J. Spacecr. Rockets* **1996**, *33*, 131−136.
(25) Andersson, M. B.; Petterson, J. B. C. Vibrational Excitation of SF_6 Scattering from Graphite. *Chem. Phys. Lett.* **1996**, *250*, 555−559.
(26) Kinefuchi, I.; Yamaguchi, H.; Shiozaki, S.; Sakiyama, Y.; Matsumoto, Y. In *Out-of-Plane Scattering Distribution of Nitrogen Molecular beam on Graphite (0001) Surface*, AIP Conference Proceedings, 2005; p 947.
(27) Oh, J.; Kondo, T.; Arakawa, K.; Saito, Y.; Nakamura, J.; Hayes, W. W.; Manson, J. R. Scattering of CO and N_2 Molecules by a Graphite Surface. *J. Phys.: Condens. Matter* **2012**, *24*, No. 354001.
(28) Oh, J.; Kondo, T.; Arakawa, K.; Saito, Y.; Hayes, W. W.; Manson, J. R.; Nakamura, J. Angular Intensity Distribution of a Molecular Oxygen Beam Scattered from a Graphite Surface. *J. Phys. Chem. A* **2011**, *115*, 7089−7095.
(29) Hayes, W. W.; Oh, J.; Kondo, T.; Arakawa, K.; Saito, Y.; Nakamura, J.; Manson, J. R. Scattering of O_2 from a Graphite Surface. *J. Phys.: Condens. Matter* **2012**, *24*, No. 104010.
(30) Watanabe, Y.; Yamaguchi, H.; Hashinokuchi, M.; Sawabe, K.; Maruyama, S.; Matsumoto, Y.; Shobatake, K. Trampoline Motions in Xe-Graphite (0001) Surface Scattering. *Chem. Phys. Lett.* **2005**, *413*, 331−334.
(31) Watanabe, Y.; Yamaguchi, H.; Hashinokuchi, M.; Sawabe, K.; Maruyama, S.; Matsumoto, Y.; Shobatake, K. Energy Transfer in Hyperthermal Xe-Graphite Surface Scattering. *Eur. Phys. J. D* **2006**, *38*, 103−109.
(32) Logan, R. M.; Stickney, R. E. Simple Classical Model for the Scattering of Gas Atoms from a Solid Surface. *J. Chem. Phys.* **1966**, *44*, 195−201.
(33) Grimmelmann, E. K.; Tully, J. C.; Cardillo, M. J. Hard-Cube Model Analysis of Gas-Surface Energy Accommodation. *J. Chem. Phys.* **1980**, *72*, 1039−1043.
(34) Majumder, M.; Bhandari, H. N.; Pratihar, S.; Hase, W. L. Chemical Dynamics Simulations of Low Energy N_2 Collisions with Graphite. *J. Phys. Chem. C* **2018**, *122*, 612−623.
(35) Gibson, K. D.; Sibener, S. J. Scattering Dynamics, Survival, and Dispersal of Dimethyl Methylphosphonate Interacting with the Surface of Multilayer Graphene. *J. Phys. Chem. A* **2016**, *120*, 4863−4871.
(36) Jorgensen, W. L.; Maxwell, D. S.; Tirado-Rives, J. Development and Testing of the OPLS All-Atom Force Field on Conformational Energetics and Properties of Organic Liquids. *J. Am. Chem. Soc.* **1996**, *118*, 11225−11236.
(37) Konowalow, D. D.; Hirschfelder, J. O. Morse Potential Parameters for O-O, N-N, and N-O Interactions. *Phys. Fluids* **1961**, *4*, 637−642.
(38) Wesolowski, T. A.; Parisel, O.; Ellinger, Y.; Weber, J. Comparative Study of Benzene···X (X = O_2, N_2, CO) Complexes Using Density Functional Theory: The Importance of an Accurate Exchange-Correlation Energy Density at High Reduced Density Gradient. *J. Phys. Chem. A* **1997**, *101*, 7818−7825.
(39) Wesołowski, T. A.; Ellinger, Y.; Weber, J. Density Functional Theory with an Approximate Kinetic Energy Functional Applied to Study Structure and Stability of Weak van der Waals Complexes. *J. Chem. Phys.* **1998**, *108*, 6078−6083.
(40) Gooding, E. A.; Serak, K. R.; Ogilby, P. R. Ground State Benzene-Oxygen Complex. *J. Phys. Chem.* **1991**, *95*, 7868−7871.

DOI: 10.1021/acs.jpcc.8b02574
J. Phys. Chem. C 2018, 122, 16048−16059

(41) Grover, J. R.; Hagenow, G.; Walters, E. A. Complexes of Oxygen with Benzene and Hexafluorobenzene. *J. Chem. Phys.* **1992**, *97*, 628−642.
(42) Granucci, G.; Persico, M. Benzene-O_2 Interaction Potential from Ab Initio Calculations. *Chem. Phys. Lett.* **1993**, *205*, 331−336.
(43) Casero, J. J.; Joens, J. A. Thermochemistry of Gas-Phase Molecular Complexes of Fluorobenzene and Toluene with Oxygen. *J. Phys. Chem. A* **1999**, *103*, 7136−7138.
(44) Casero, J. J.; Joens, J. A. Thermochemistry of Gas Phase Molecular Complexes of Benzene with Oxygen. *J. Phys. Chem. A* **1997**, *101*, 2607−2609.
(45) Mehta, N. A.; Murray, V. J.; Xu, C.; Levin, D. A.; Minton, T. K. Nonreactive Scattering of N2 from Layered Graphene Using Molecular Beam Experiments and Molecular Dynamics. *J. Phys. Chem. C* **2018**, *122*, 9859−9874.
(46) Hu, X.; Hase, W. L.; Pirraglia, T. Vectorization of the General Monte Carlo Classical Trajectory Program VENUS. *J. Comput. Chem.* **1991**, *12*, 1014−1024.
(47) Hase, W. L.; Duchovic, R. J.; Hu, X.; Komornicki, A.; Lim, K. F.; Lu, D.-H.; Peslherbe, G. H.; Swamy, K. N.; Vande Linde, S. R.; Varandas, A.; Wang, H.; Wolf, R. J. VENUS96: A general chemical dynamics computer program. *Quantum Chem. Program Exch. Bull.* **1996**, *16*, No. 671.
(48) Gutzwiller, M. C. *Chaos in Classical and Quantum Mechanics*; Springer Verlag: New York, 1990.
(49) Martínez-Núñez, E.; Rahaman, A.; Hase, W. L. Chemical Dynamics Simulations of CO_2 Scattering on a Fluorinated Self-Assembled Monolayer Surface. *J. Phys. Chem. C* **2007**, *111*, 354−364.
(50) Barnes, G. L.; Hase, W. L. Energy Transfer, Unfolding, and Fragmentation Dynamics in Collisions of N-Protonated Octaglycine with an H-SAM Surface. *J. Am. Chem. Soc.* **2009**, *131*, 17185−17139.
(51) Peng, Y.; Liu, L.; Cao, Z.; Li, S.; Mazyar, O. A.; Hase, W. L.; Yan, T. Chemical Dynamics Simulation of Ne Atom Scattering off a Squalane Surface. *J. Phys. Chem. C* **2008**, *112*, 20340−20346.
(52) Tasić, U.; Day, B. S.; Yan, T.; Morris, J. R.; Hase, W. L. Chemical Dynamics Study of Intrasurface Hydrogen-Bonding Effects in Gas-Surface Energy Exchange and Accomodation. *J. Phys. Chem. C* **2008**, *112*, 476−490.
(53) Head-Gordon, M.; Tully, J. C.; Rettner, C. T.; Mullins, C. B.; Auerbach, D. J. On the Nature of Trapping and Desorption at High Surface Temperatures. Theory and Experiments for the Ar-Pt(111) System. *J. Chem. Phys.* **1991**, *94*, 1516−1527.
(54) Smith, J. N., Jr. Molecular Beam Scattering from Solid Surfaces: A Critical Review. *Surf. Sci.* **1973**, *34*, 613−637.
(55) Yan, T.; Isa, N.; Gibson, K. D.; Sibener, S. J.; Hase, W. L. Role of Surface Intramolecular Dynamics in the Efficiency of Energy Transfer in Collisions with a n-Hexylthiolate Self-Assembled Monolayer. *J. Phys. Chem. A* **2003**, *107*, 10600−10607.
(56) Yan, T.-Y.; Hase, W. L.; Barker, J. R. Identifying Trapping Desorption in Gas-Surface Scattering. *Chem. Phys. Lett.* **2000**, *329*, 84−91.
(57) Yan, T.-Y.; Hase, W. L. A Hamiltonian with a Subset of Normal Modes for Studying Mode Specific Energy Transfer in Intermolecular Collisions. *J. Phys. Chem. A* **2001**, *105*, 2617−2625.
(58) Rahaman, A.; Zhou, J. B.; Hase, W. L. Effects of Projectile Orientation and Surface Impact Site on the Efficiency Projectile Excitation in Surface Induced Dissociation. Protonated Diglycine Collisions with Diamond {111}. *Int. J. Mass Spectrom.* **2006**, *249−250*, 321−329.

DOI: 10.1021/acs.jpcc.8b02574
J. Phys. Chem. C 2018, 122, 16048−16059